Scientific Journal of Silesian University of Technology. Series Transport
Zeszyty Naukowe Politechniki Śląskiej. Seria Transport

Volume 131 **2026**

p-ISSN: 0209-3324

e-ISSN: 2450-1549

DOI: https://doi.org/10.20858/sjsutst.2026.131.4

Journal homepage: http://sjsutst.polsl.pl

Article citation information:
Elmaihy, A., Abd El-Latif, M. Performance and sizing of PEM fuel cells under variable operating conditions for an autonomous underwater vehicle. *Scientific Journal of Silesian University of Technology. Series Transport*. 2026, **131**, 63-87. ISSN: 0209-3324. DOI: https://doi.org/10.20858/sjsutst.2026.131.4

Ali ELMAIHY[1], Mohamed ABD El-LATIF[2]

PERFORMANCE AND SIZING OF PEM FUEL CELLS UNDER VARIABLE OPERATING CONDITIONS FOR AN AUTONOMOUS UNDERWATER VEHICLE

Summary. Ensuring a reliable power supply is a key challenge for autonomous underwater vehicles (AUVs), especially when deeper diving, longer endurance, and extended mission range are required. Proton exchange membrane (PEM) fuel cells offer a promising solution due to their high-energy density and quiet operation. This study conducted a detailed PEM fuel cell model in MATLAB/Simulink to evaluate how operating conditions affect single-cell electrochemical behavior and stack-level sizing. The model incorporates activation and ohmic losses to quantify variations in cell voltage under different temperatures and reactant supply pressures. Based on these analyses, performance and sizing indices are derived for a practical AUV power system. Results indicate that increasing operating temperature from 55°C to 85°C, together with increasing oxygen and hydrogen supply pressures from 1 to 3 atm, enables a 20% reduction in the required number of cells, directly translating into similar reductions in stack mass and volume. Moreover, reactant consumption decreases by 9.5%, improving overall energy efficiency by 9.6%. These findings demonstrate the strong influence of operating

[1] Faculty Department of Ships and Submarines, Military Technical College, Egypt. Email: ali.elmaihy@mtc.edu.eg. ORCID: https://orcid.org/0000-0002-3917-9533
[2] Faculty of Mechanical Design and Production Department, Military Technical College, Egypt. Email: abdelmenim@mtc.edu.eg. ORCID: https://orcid.org/0009-0007-4658-4530

conditions on PEM fuel cell performance and provide guidelines for optimized sizing of AUV fuel cell power systems.

Keywords: fuel cell performance, activation over potential, ohmic losses, operating temperature, supply pressures, AUV

1. INTRODUCTION

Underwater vehicles, including miniature submarines and autonomous underwater vehicles (AUVs), are increasingly used in the military and commercial fields. Similar to AUVs, the power system of AUVs has high requirements for stealth (without vibration and noise) and long endurance [1]. Because of their low pollution and energy efficiency, fuel cell vehicles (FCVs) have gained popularity in response to growing worries about global warming, pollution, and energy consumption [2].

PEMFC and solid oxide fuel cells (SOFC) can be utilized for AUVs [3,4]. PEMFC is the recommended option since it performs better and runs at lower temperatures (below 100°C). Many AUVs currently run on batteries [5], but AUV endurance will increase with the adoption of fuel cell systems [6,7]. Because the storage media in fuel cells have a far higher energy density than batteries, they can outperform them in terms of energy density; nonetheless, the issues arise from their weights and system sizes [8].

Recent research indicates that commercial AUVs use batteries to store power. Battery-powered AUVs with greater endurance and range are significantly bigger than regular ones, which reduces their utility and increases their space requirements [5,9]. So, fuel cells are used in the AUV industry. According to [10], the properties of suitable fuel cell systems are:

1. The size of fuel cell systems must be as small and as light as possible.
2. The power output of fuel cell systems must be in the range of 1 kW to 2 kW.
3. Fuel cell systems should be removable, exchangeable, and replaceable.

The integration of fuel cell technology into Autonomous Underwater Vehicles for naval applications presents a compelling avenue for enhanced operational capabilities, characterized by extended endurance, reduced acoustic signatures, and improved energy efficiency [11]. However, the realization of these benefits hinges critically on a comprehensive understanding of the intricate relationship between fuel cell operating conditions, system size, and overall performance within the unique constraints imposed by the underwater environment. AUVs represent a paradigm shift in underwater exploration and data acquisition, offering unparalleled maneuverability and the ability to access remote and complex underwater environments without direct human intervention [12]. The evolution of AUV technology has been driven by advancements in control systems, communication protocols, and sensory technologies, enabling increasingly sophisticated missions in challenging underwater settings [13]. The operational demands of AUVs in naval contexts are particularly stringent, necessitating robust performance under varying environmental conditions, including temperature fluctuations, pressure variations, and exposure to corrosive seawater [14].

The performance of fuel cells is intricately linked to various operating conditions, encompassing temperature, pressure, humidity, and reactant stoichiometry, all of which exert a significant influence on the electrochemical reaction kinetics, mass transport phenomena, and membrane properties within the fuel cell stack. Hydrogen energy systems, particularly those employing PEM fuel cells, have been reviewed for underwater applications, emphasizing the importance of storage methods and operating parameters in system design [9]. The literature

indicates that hydrogen/oxygen storage strategies and fuel cell operating conditions are interconnected factors that determine the overall system size and performance. Proper management of these parameters can lead to more compact and efficient fuel cell systems suitable for AUV deployment [9]. Knyazhev and Loshchenkov [15] review various fuel cell types, emphasizing their performance under different operating conditions. It highlights how these conditions affect size and efficiency, making them suitable for naval AUV applications, ensuring extended operational duration and enhanced cruising range. Mendez et al. [16,17] discussed that fuel cell operating conditions significantly influence size and performance, emphasizing the need for compact, efficient systems. It highlights the importance of optimizing reactant storage and system configurations to enhance endurance and efficiency in AUV applications. Pielecha [18] analyzed fuel cell performance under various driving conditions, highlighting that urban, rural, and motorway scenarios significantly affect power output and losses. It emphasizes the importance of optimizing operating conditions to enhance fuel cell efficiency and longevity in applications like AUVs. Tsukioka et al. [19] discussed that fuel cell size and performance in AUVs are influenced by operating conditions such as temperature, pressure, and the number of cells in series, which determine output voltage and efficiency, impacting overall energy generation and operational capability. Challenges associated with hydrogen fuel cells in transportation and underwater environments further underscore the necessity of optimizing operating conditions. These include issues related to durability, efficiency, and system integration, which are directly impacted by temperature, humidity, and load fluctuations [20]. Addressing these challenges through advanced energy management strategies, such as high-fidelity simulation models combined with experimental data, has shown promise in enhancing performance and reducing system size [21].

Because PEMFC systems are complex, multimodal, and intricately linked, modeling their properties for design and performance assessment is difficult. Over the years, significant progress has been made in comprehending the behavior of PEMFC features using mathematical modeling [22-34]. Models of integrated cars with fuel cell stacks are necessary to examine the system behavior under varied load, reagent gas pressure, and temperature conditions in order to maximize the utilization of PEMFCs [35]. In the meantime, modeling is becoming more and more significant in design, analysis, and performance evaluation. Qasem and Abdulrahman [36] reported that, despite several modeling approaches used in literature for the prediction of PEMFCs performance, Amphlett et al.'s mathematical modeling [37,38] was recognized for its prediction accuracy under different operating conditions. The majority of models in the literature are supported by experimental work. Evaluating and comparing the polarization curve derived from both mathematical and experimental investigations is the most popular validation method. If the findings of two polarization curves are the same or nearly identical, the model is reliable [39].

The objective of this paper is to use MATLAB Simulink to build a fuel cell model according to [37,38]. Then, select a well-known AUV to ascertain its power needs. The final result was a block diagram that forms the basis for forecasting the fuel cell's performance under various operating circumstances. The second part of the paper investigates the impact of operating conditions on the sizing of the fuel cell system, as well as the consumption rates of hydrogen and oxygen, which play a crucial role in determining the overall endurance of the AUV.

2. FUEL CELL MODEL DESCRIPTION

An electrochemical model that can be used to predict the behavior of PEMFC is presented in this section. The optimal simulation results depend on the definition of a set of parameters used in this mathematical model. The following expression can be used to define the output voltage of a single cell, V_{cell} [22,37,38].

$$V_{cell} = E_{Nernst} + \eta_{Ohmic} + \eta_{Act} \tag{1}$$

Where E_{Nernst} is the Nernst equation, which is an expression for the electromotive force (EMF) for a given product; η_{Act} is the activation overvoltage, which is the amount of voltage used to drive the reaction; η_{Ohmic} is the ohmic overvoltage, which is the amount of voltage lost to the resistance to electron flow in the electrodes and the resistance to ion flow in the electrolyte; the terms of Eq. 1 are discussed in the following sections.

2.1. Nernst Voltage

The Nernst equation for the reaction described above:

$$E_{Nernst} = 1.229 - 0.85 \text{ x } 10^{-3} \text{ x } (T - 298.15) + 4.3085\text{x}10^{-5} \text{ x } T \text{ x } (log(P_{H2}^{*}) + 0.5 \text{ x } log(P_{O2}^{*})) \tag{2}$$

Where T is the stack temperature in (K), and P_{H2}^{*} and P_{O2}^{*} are the hydrogen and oxygen partial gas pressures in (atm) at the surface of the catalyst at the anode and cathode, respectively. At each electrode, two distinct cases need to be taken into account (for example, the first has an inert diluent in the input flows, either carbon dioxide in the anode flow or nitrogen in the cathode flow), which will not be considered here. The flows in the second scenario don't contain any diluent. So P_{H2}^{*} and P_{O2}^{*} will be described as [37].

The first case: diluted H_2 and O_2:

$$P_{H_2}^{*} = P_{Anode} \times \left(1 - \left(0.5 \times x_{H_2O}^{Anode}\right) - \left(X_{CO_2}^{channel} \times e^{\left(\frac{0.183 \times i}{\left(T^{(0.832)}\right)}\right)} \right) \right) \tag{3}$$

$$P_{O_2}^{*} = P_{Cathode} \times \left(1 - x_{H_2O}^{Cathode} - X_{N_2}^{channel} \times e^{\left(\frac{0.291 \times i}{T^{(0.882)}}\right)} \right) \tag{4}$$

Where i is the current density ($i = I/A_{cell}$ $[A/m^2]$). P_{Anode} and $P_{Cathode}$ are the total humid gas pressures at both the anode and the cathode, and are given by:

$$P_{Anode} = P_{Anode}^{Dry} + 0.5 \times P_{H_2O}^{sat} \tag{5}$$

$$P_{Cathode} = P_{Cathode}^{Dry} + P_{H_2O}^{sat} \tag{6}$$

Where P_{Anode}^{Dry} and $P_{Cathode}^{Dry}$ are the total dry gas pressures at both the anode and the cathode. $X_{H_2O}^{anode}$ and $X_{H_2O}^{Cathode}$ are the molar fractions of water in a gas stream at anode and cathode, respectively, at saturation condition for a given temperature, and are given by:

$$X_{H_2O}^{Anode} = 0.5 \times \left(P_{H_2O}^{sat}/P_{Anode}\right) \tag{7}$$

$$X_{H_2O}^{Cathode} = \left(P_{H_2O}^{sat}/P_{Cathode}\right) \tag{8}$$

The $P_{H_2O}^{sat}$ term is the saturation pressure of water at the operating temperature *T*. It is determined in a fuel cell by the following empirical equation:

$$P_{H_2O}^{sat} = e^{\left(70.434643-\left(\frac{7362.6981}{T}\right)+(0.006952085\times T)-\left(9\times log(T)\right)\right)} \tag{9}$$

$X_{N_2}^{channel}$ and $X_{CO_2}^{channel}$ are the average molar fractions of nitrogen in the air stream and carbon dioxide in the hydrogen stream, respectively, and are given by:

$$X_{N_2}^{Channel} = \left(\frac{X_{N_{2,Humid}}^{out}-X_{N_{2,Humid}}^{in}}{\left(log\left(\frac{X_{N_{2,Humid}}^{out}}{X_{N_{2,Humid}}^{in}}\right)\right)}\right) \tag{10}$$

$$X_{CO_2}^{Channel} = \left(\frac{X_{CO_2}^{in}-X_{CO_2}^{out}}{log\left(\frac{X_{CO_2}^{in}}{X_{CO_2}^{out}}\right)}\right) \tag{11}$$

$X_{N_{2,Humid}}^{out}$ and $X_{N_{2,Humid}}^{in}$ are the mole fractions of inlet and outlet N_2 in the mixture of oxygen and nitrogen, saturated with water vapor, given by:

$$X_{N_2,Humid}^{out} = \left(\frac{\left(1-X_{H_2O}^{Cathodet}\right)}{\left(1+\left(\frac{(SR_1-1)}{SR_1}\right)\times\left(\frac{X_{O_2}}{\left(1-X_{O_2}\right)}\right)\right)}\right) \tag{12}$$

$$X_{N_2,Humid}^{in} = \left(1 - X_{H_2O}^{Cathodet}\right) \times X_{N_2,Dry}^{in} \tag{13}$$

$X_{CO_2}^{in}$ and $X_{CO_2}^{out}$ are the mole fractions of inlet and outlet CO_2 in the mixture of Hydrogen and carbon dioxide, and given by:

$$X_{CO_2}^{in} = \left(1 - X_{H_2}\right) \times \left(1 - X_{H_2O}^{Anode}\right) \tag{14}$$

$$X_{CO_2}^{out} = \left(\frac{\left(1 - X_{H_2O}^{Anode}\right)}{\left(1 + \left(\frac{SR_2 - 1}{SR_2}\right)\right)} \times \left(\frac{X_{H_2}}{\left(1 - X_{H_2}\right)} \right) \right) \quad (15)$$

SR_1 and SR_2 are the stoichiometric ratios of oxygen and hydrogen, respectively. X_{O_2} and X_{H_2} are the mole fractions of O_2 and H_2 on the cathode and anode streams, respectively.

The second case: Pure inlet streams of H_2 and O_2:

$$P_{H_2}^{*} = P_{H_2O}^{sat} \times \left(\frac{1}{exp\left(\frac{4.192 \times i}{T^{1.334}}\right).x_{H_2O}^{Anode}} - 1 \right) \quad (16)$$

$$P_{O_2}^{*} = 0.5 P_{H_2O}^{sat} \times \left(\frac{1}{exp\left(\frac{1.6532 \times i}{T^{1.334}}\right).x_{H_2O}^{Cathode}} - 1 \right) \quad (17)$$

2.2. Activation overvoltage

Activation losses (also called activation overpotentials) arise from the energy barrier that must be overcome for the electrochemical reactions to occur at the electrodes. These losses are more significant at low current densities. The loss can be decreased if steps are taken to increase the reaction rates by increasing the temperature or pressure in the fuel cell, which operates in a temperature range of approximately 55°C to 85°C. The semi-empirical equation for the activation overvoltage is given by [37,38]:

$$\eta_{act} = \left(-0.9514 + 0.00312 \times T + 7.4 \times 10^{-5} \times T \times \left(log(C_{O2}^{*}) \right) - 0.00187 \times T\left(log(\mathrm{I}) \right) \right) \quad (18)$$

Where the concentration of dissolved oxygen at the gas/liquid interface(C_{O2}^{*}) can be defined by a Henry's law expression of the form:

$$C_{O2}^{*} = \frac{P_{O2}^{*}}{\left(5.08 \times 10^{6} \times e^{\left(-489/T\right)}\right)} \quad (19)$$

Where the expression for $P_{O2}^{*}$is given by Eq. 2.

2.3. Ohmic Overvoltage

Another portion of the voltage generated by the electrochemical reaction is lost due to the resistance to electron flow in the electrodes and graphite collector plates, and the resistance to ion flow in the electrolyte. The ohmic losses can be reduced by using thin, well-hydrated membranes with high proton conductivity, improving electrical contact, and using materials with low resistivity, and maintaining proper membrane hydration (dry membranes increase resistance). The ohmic overvoltage can be expressed following Ohm's law as:

$$\eta_{ohmic} = -(R_{internal} \times I) \quad (20)$$

Where $R_{internal}$ is the resistance to electron transfer and is calculated by:

$$R_{internal} = 0.01605 - 3.5 \times 10^{-5} \times T + 8 \times 10^{-5} \times I \quad (21)$$

2.4. Fuel Cell Model Implementation

In this paper, MATLAB/Simulink is used to set up the PEMFC system model. Simulink is a software package for modeling and simulation, which can be used to evaluate the system performance and optimize the system design. (Figure 1) shows the Simulink model of the simulation diagram of the PEMFC dynamic model based on Eqs (1) to (21).

3. MODEL VALIDATION

To validate the model, a single cell, the Ballard Mark IV model, was simulated and fed with gases H_2 and O_2. For oxygen, the dry-basis mole fraction, X_{O_2}, settings were 0.21, 0.46, and 1.00; for hydrogen, X_{H_2}, they were 0.65, 0.81, and 1.00. By keeping the total dry gas pressure at the cathode and anode P_{Anode}^{Dry} and $P_{Cathode}^{Dry}$constant at 3.06 atm abs, the partial pressure settings were accomplished. The stoichiometries of the input flows were maintained at 1.73 cm^3 of fuel (anode gas) for every cm^3 of hydrogen consumed and 8.33 cm^3 of oxidant (cathode gas) per cm^3 of oxygen used throughout all runs. The stoichiometric ratios SR_1 and SR_2 are calculated for validation by:

$$SR_1 = 8.33 \times X_{O_2} \quad (22)$$

$$SR_2 = 1.73 \times X_{H_2} \quad (23)$$

The inlet dry partial pressure:

$$P_{H_2}^{in,\ Dry} = X_{H_2} P_{Anode}^{Dry} \quad (24)$$

$$P_{O_2}^{in,\ Dry} = X_{O_2} P_{Cathode}^{Dry} \quad (25)$$

The Mark IV employs a Nafion membrane (0.18 mm in thickness), with an active surface area of 50.56 cm^2. Table 1 displays the experimental settings of 28 runs with the corresponding measured parameters and corresponding predicted results. Comparing diagrams of the total output voltage, fuel cell resistance, and activation overvoltage between the model predictions and the experimental data [38] are presented in Figures 2 to 4, respectively. Calculated output voltage response to a range of independent operating current, temperature, and oxygen partial pressure variations, as shown in the experimental settings shown in Table 1.

It is demonstrated that the model accurately predicts fuel cell voltage for current densities as high as 0.33 A/cm^2 in the temperature range of 55 to 85 degrees Celsius and correlates fuel cell voltage over the experimental range of current densities. In conclusion, the modeling strategy is found to be successful, efficient, and simple to use with a limited quantity of data.

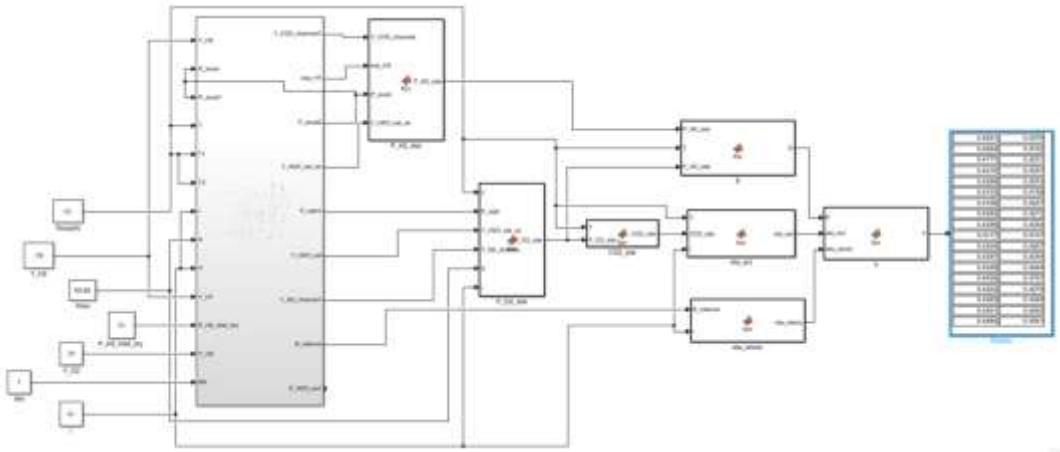

Fig. 1. The block diagram of the MATLAB/SIMULINK model of PEMFCs

Tab. 1
Experimental settings and comparison between measured values and predicted results

Experimental setting					Measured Results		Predicted results		% Error	
Run No.	T [K]	I [Amp]	X_{O_2}	X_{H_2}	V_{cell} [volt]	R_{int} [Ω]	V_{cell} [volt]	R_{int} [Ω]	V_{cell}	R_{int}
1	358	2.72	0.46	0.81	0.91	0.00388	0.916	0.00374	-0.66	3.61
2	328	6.66	0.21	0.81	0.773	0.00489	0.775	0.00510	-0.26	-4.29
3	343	6.66	0.46	0.81	0.82	0.00455	0.823	0.00458	-0.37	-0.66
4	358	6.66	1	0.81	0.867	0.0041	0.869	0.00405	-0.23	1.22
5	343	6.66	1	1	0.851	0.00453	0.856	0.00458	-0.59	-1.10
6	343	6.66	0.21	0.65	0.781	0.00455	0.784	0.00458	-0.38	-0.66
7	328	6.66	0.46	0.65	0.802	0.00489	0.800	0.00510	0.25	-4.29
8	343	2.72	0.21	0.81	0.863	0.0042	0.867	0.00426	-0.46	-1.43
9	343	6.66	0.46	0.81	0.824	0.00446	0.823	0.00458	0.12	-2.69
10	343	6.66	0.46	0.81	0.827	0.00441	0.823	0.00458	0.48	-3.85
11	328	2.72	0.46	0.81	0.888	0.00495	0.882	0.00479	0.68	3.23
12	328	6.66	1	0.81	0.835	0.00505	0.833	0.00510	0.24	-0.99
13	343	6.66	0.46	0.81	0.826	0.00437	0.823	0.00458	0.36	-4.81
14	358	6.66	0.21	0.81	0.809	0.00406	0.805	0.00405	0.49	0.25
15	358	6.66	0.46	1	0.846	0.00393	0.844	0.00405	0.24	-3.05
16	358	6.66	0.46	0.65	0.836	0.00399	0.833	0.00405	0.36	-1.50
17	343	16.33	0.46	1	0.715	0.00477	0.713	0.00535	0.28	-12.16
18	343	16.33	1	0.81	0.73	0.00493	0.736	0.00535	-0.82	-8.52
19	343	6.66	0.46	0.81	0.823	0.00456	0.823	0.00458	0.00	-0.44
20	343	6.66	0.21	0.81	0.792	0.00441	0.790	0.00458	0.25	-3.85
21	358	16.33	0.46	0.81	0.729	0.00442	0.727	0.00483	0.27	-9.28
22	343	2.72	0.46	1	0.901	0.00428	0.904	0.00426	-0.33	0.47
23	343	6.66	1	0.65	0.847	0.00444	0.844	0.00458	0.35	-3.15
24	343	2.72	0.46	0.65	0.898	0.00428	0.893	0.00426	0.56	0.47
25	343	16.33	0.21	0.81	0.662	0.00477	0.676	0.00535	-2.11	-12.16
26	343	6.66	0.46	0.81	0.822	0.00456	0.823	0.00458	-0.12	-0.44
27	328	6.66	0.46	1	0.807	0.00502	0.812	0.00510	-0.62	-1.59
28	343	16.33	0.46	0.65	0.7	0.0049	0.702	0.00535	-0.29	-9.18

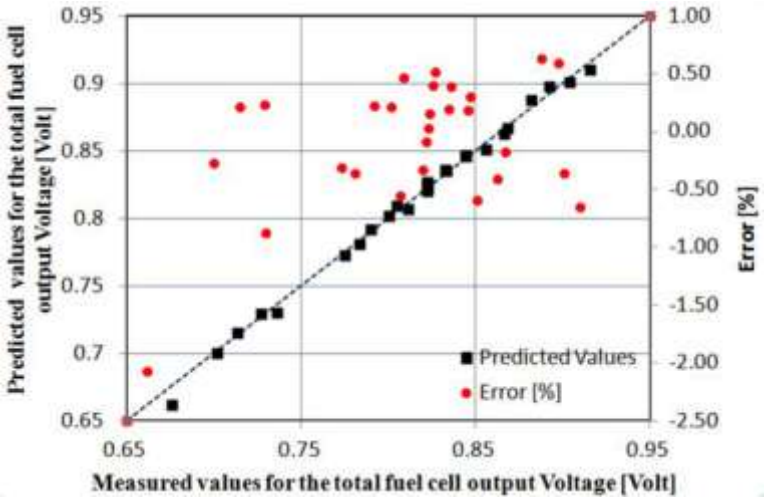

Fig. 2. Parity plot of the model prediction and the measured values for the total output voltage

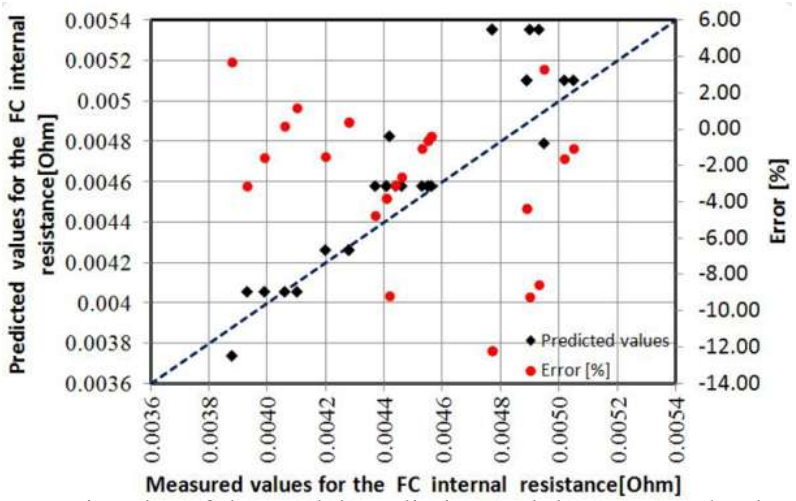

Fig. 3. Parity plot of the model prediction and the measured values for the FC internal resistance

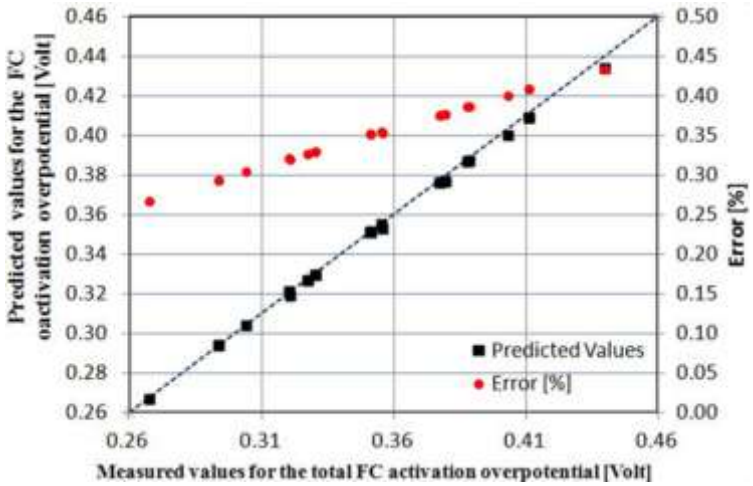

Fig. 4. Parity plot of the model prediction and the measured values for the FC activation overpotential

4. METHODOLOGY

This section aims to present a procedure for obtaining the most suitable operating conditions for the fuel cell to power an AUV. The inferred requirements of FCs for AUVs are mentioned in [5]. The proposed procedure is summarized as follows:

1. Selection of the AUV.
2. Estimation of the required power for the selected AUV.
3. Prediction of the performance of one cell of Ballard IV FC (cell output voltage and power) at different operating conditions, namely, Cell temperature, H_2 supply pressure, and O_2 supply pressure at different current densities.
4. Recording the maximum power and the corresponding current density for each operating condition ($P_{O_2}^{in}$, $P_{H_2}^{in}$ and T).
5. Calculations of the number of cells needed to produce the AUV's required power at each operating condition.
6. Calculation of the H_2 and O_2 consumption,
7. Calculation of the FC efficiency.
8. Analysis of the obtained results.

Figure 5 presents a flowchart illustrating the previously described procedures.

4.1. AUV Selection and Required Power Estimation

The AUV ECA A27-E [5,40] is a Classical rear propeller with control surface architectures, such as in large conventional submarines equipped with rudders, which take an important place in the AUV market since it has a great performance following straight lines due to its torpedo-shaped hull. The main characteristics of A27-E AUV are shown in Table 2.

The viscous resistance coefficient C_V, the friction resistance coefficient C_F, and the shape factor ($1+k$) are used to calculate the power consumption of propulsion engines.

C_F can be calculated using the International Towing Tank Conference 57 correlation line (ITTC, 1957) [41]:

$$C_F = \frac{0.075}{(log_{10}Re-2)^2} \tag{26}$$

Where Re is the Reynolds Number based on the AUV length and speed:

$$Re=\frac{vL}{\mu} \tag{27}$$

Where: μ is the kinematic viscosity of seawater [m^2/s]; L is the length of ROV [m]; v is the calculated speed of ROV [m/s]. For AUVs with a circular cross-section, Droblenkov's curve can be used to determine the form coefficient:

$$(1+k) = 1 + 0.2(D/L) + 8(D/L)^2 - 10(D/L)^3 \tag{28}$$

Thus, viscous resistance is calculated by the expression:

$$R_v = \frac{1}{2}\rho A v^2 C_f (1+K) \tag{29}$$

Where: ρ = 1025 [kg/m^3]- density of seawater; A is the wet surface area of the *ROV*, calculated as a cylinder of diameter D and length L. The required thrust power is calculated by:

$$\dot{W}_{AUV} = \left(\frac{1}{\eta_D}\rho A C_f (1+K)\right) v^3 \tag{30}$$

Where η_D is the propeller thrust performance.

Figure 6 shows the dependence of AUV resistance and required thrust power on the AUV speed. At the maximum AUV speed, the required thrust power is 1523 W.

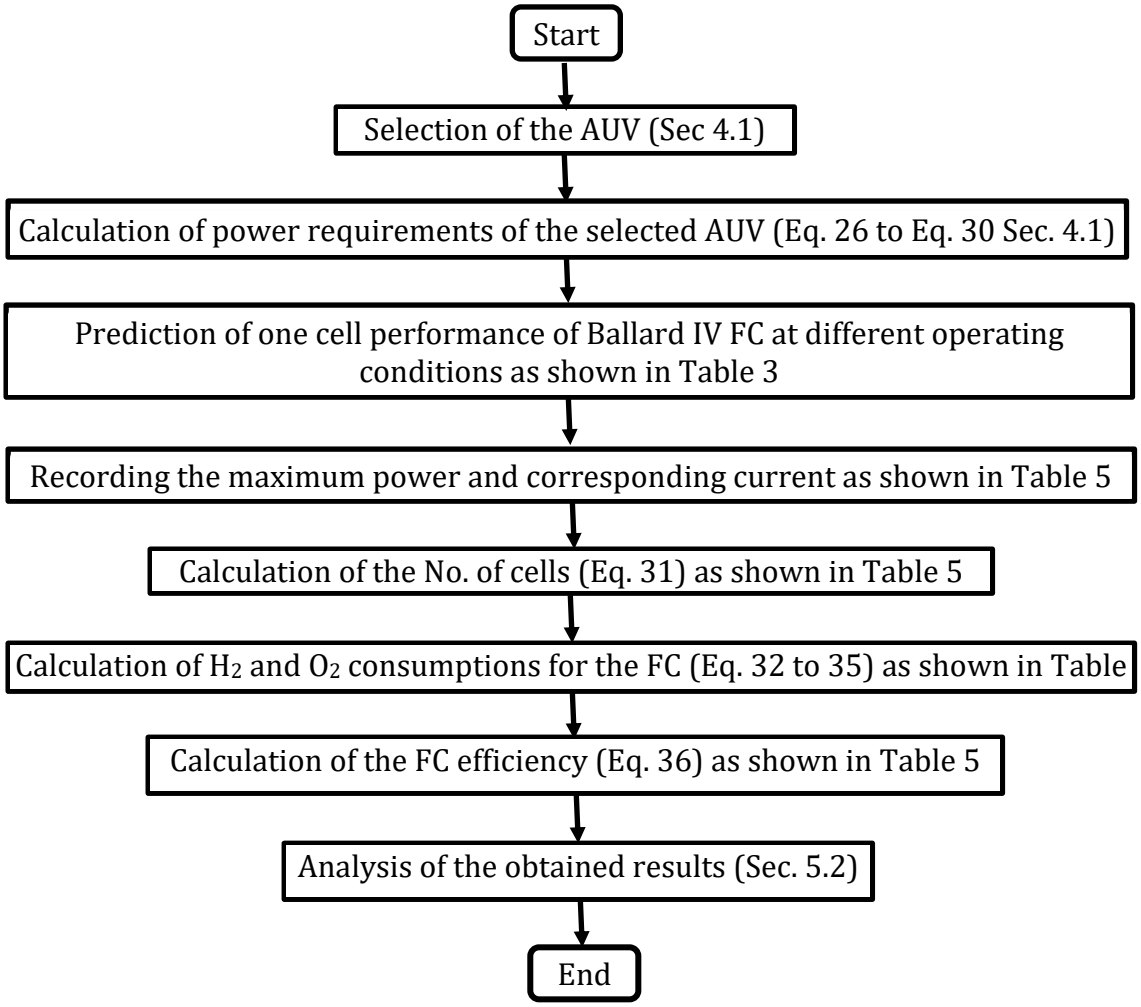

Fig. 5. Flow diagram of the method presented for sizing the AUV fuel cell and calculating the gas consumption at different operating conditions

Tab. 2

Main Characteristics of A27-E AUV [5]

Parameters	Value
Length	4.5 m
Diameter	0.73 m

Weight	850 kg
Maximum diving depth	300 m
Maximum speed	6 knotes-3.09 m/s
Underwater endurance at speed 6 knots	30 hr

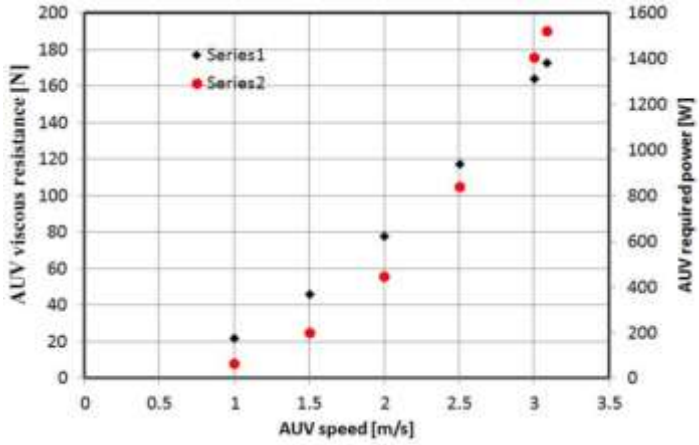

Fig. 6. Viscous resistance power requirement at different AUV speeds

4.2. Single FC at different operating conditions

The mathematical model described in Section II is used to predict the performance of one cell of Ballard IV FC at different operating conditions. Pure oxygen systems are usually exclusively utilized in situations when air is unavailable, such as submarines and other vessels, due to technical challenges, the additional bulk and weight of air storage, and associated safety considerations [42].

The operating conditions selected in this study are consistent with those commonly reported for PEM fuel cells used in AUV and underwater applications. Specifically, the temperature range of 55-85°C aligns with the operating range of PEM fuel cells [10,11, 27] and the typical operating window of Nafion-based PEM fuel cells (60-80°C), where high proton conductivity and stable membrane performance are achieved [25]. Similarly, the selected hydrogen and oxygen inlet pressures (1-3 atm) fall within the commonly adopted range in the literature [27], where moderate pressurization improves reactant availability and reduces mass transport losses without imposing excessive compression penalties or safety risks, as discussed in [43]. Therefore, these ranges represent a practical compromise between performance, efficiency, system compactness, and operational safety, making them suitable for AUV applications and consistent with established literature.

Table 3 shows 36 combinations of different operating conditions with a special designation that is developed to enable straightforward identification and correlation with the operating conditions. The designation is OIHJTM where O is for oxygen, I is the inlet dry pressure of O_2 [atom], H is for hydrogen, J is inlet dry pressure of H_2 [atom], T is for operating cell temperature and M is the value of the temperature [^{o}C] so O1H3T60 means a case in which the inlet oxygen dry pressure is 1 atom, the inlet hydrogen dry pressure is 3 atoms operating at 60^{o}C. The stoichiometric ratios SR_1 and SR_2 are fixed at 1.4 and 1.25 for oxygen and hydrogen, respectively, for all runs as recommended by [42].

Tab. 3

Different Calculations Operating Conditions

Case	$P_{O_2}^{in}$	$P_{H_2}^{in}$	T[K]	Case	$P_{O_2}^{in}$	$P_{H_2}^{in}$	T[K]
O1H1T55	1	1	55	O1H1T75	1	1	75
O1H2T55	1	2	55	O1H2T75	1	2	75
O1H3T55	1	3	55	O1H3T75	1	3	75
O2H1T55	2	1	55	O2H1T75	2	1	75
O2H2T55	2	2	55	O2H2T75	2	2	75
O2H3T55	2	3	55	O2H3T75	2	3	75
O3H1T55	3	1	55	O3H1T75	3	1	75
O3H2T55	3	2	55	O3H2T75	3	2	75
O3H3T55	3	3	55	O3H3T75	3	3	75
O1H1T65	1	1	65	O1H1T85	1	1	85
O1H2T65	1	2	65	O1H2T85	1	2	85
O1H3T65	1	3	65	O1H3T85	1	3	85
O2H1T65	2	1	65	O2H1T85	2	1	85
O2H2T65	2	2	65	O2H2T85	2	2	85
O2H3T65	2	3	65	O2H3T85	2	3	85
O3H1T65	3	1	65	O3H1T85	3	1	85
O3H2T65	3	2	65	O3H2T85	3	2	85
O3H3T65	3	3	65	O3H3T85	3	3	85

4.3. Fuel Cell Stack for AUV

Using the polarization curve V-I and the power curve $\dot{W}_{FC}$-I for each operating condition, the maximum power for the single FC, $\dot{W}_{FC,max}$, is determined with the corresponding current density and output voltage.

The number of cells, $N_{FC,}$ is determined by:

$$N_{FC} = \frac{\dot{W}_{AUV}}{\dot{W}_{FC,max}} \tag{31}$$

According to the electrochemical reactions of the PEMFC, the molar consumption of H_2 and O_2 can be determined as follows.

$$\dot{n}_{H_2} = \frac{SR_2 N_{FC} I}{(2F)} \tag{32}$$

$$\dot{n}_{O_2} = \frac{SR_1 N_{FC} I}{(4F)} \tag{33}$$

The inlet mass flow rate of H_2 and O_2 in gm/s is calculated by:

$$\dot{m}_{H_2} = \dot{n}_{H_2}.M_{H_2} \tag{34}$$

$$\dot{m}_{O_2} = \dot{n}_{O_2}.M_{O_2} \tag{35}$$

Where M_{H_2} and M_{O_2} are the molar masses of hydrogen and oxygen.
The fuel cell energy efficiency is calculated by [44]:

$$\eta_{FC} = \frac{N_{FC} \times \dot{W}_{FC,max}}{\dot{n}_{H_2} \times HHV_{H_2}} \tag{36}$$

5. RESULTS and DISCUSSIONS

5.1. Single FC at Different Operating Conditions

The impact of operating supply pressure of H_2 and O_2 on PEMFC performance is assessed and displayed in Figures 7 to 11. Anode and cathode gas supply conditions are examined under various combinations of $P_{O_2}^{in}$ and $P_{H_2}^{in}$ as shown in Table 3. The maximum power for all cases occurs at a current range of 36.5 A and 41.75 A, corresponding to a current density of 0.72 A/cm^2 and 0.83 A/cm^2, respectively. The output voltage and power at a current of 40 A are displayed in Table 4 and will be used for comparisons. Table 4 demonstrates the output cell voltage and power at 40 A and operating temperatures of 55°C and 85°C.

Tab. 4
The output cell voltage and power at 40 A and operating temperatures of 55°C and 85°C

Case	$P_{O_2}^{in}$	$P_{H_2}^{in}$	T[K]	V [V]	$\dot{W}_{FC}$[W]	Case	$P_{O_2}^{in}$	$P_{H_2}^{in}$	T[K]	V_{cell}[V]	$\dot{W}_{FC}$[W]
O1H1T55	1	1	55	0.401	16.043	O1H1T85	1	1	85	0.458	18.308
O1H2T55	1	2	55	0.411	16.424	O1H2T85	1	2	85	0.467	18.696
O1H3T55	1	3	55	0.416	16.650	O1H3T85	1	3	85	0.473	18.933
O2H1T55	2	1	55	0.423	16.912	O2H1T85	2	1	85	0.481	19.257
O2H2T55	2	2	55	0.432	17.293	O2H2T85	2	2	85	0.491	19.645
O2H3T55	2	3	55	0.438	17.519	O2H3T85	2	3	85	0.497	19.881
O3H1T55	3	1	55	0.436	17.421	O3H1T85	3	1	85	0.495	19.812
O3H2T55	3	2	55	0.445	17.802	O3H2T85	3	2	85	0.505	20.200
O3H3T55	3	3	55	0.451	18.027	O3H3T85	3	3	85	0.511	20.436

Examining how voltage loss responds could help explain the improvement in cell performance. The activation overpotential does not exhibit a pressure term. Activation losses are the voltage losses due to the finite kinetics of the electrochemical reactions at both electrodes, namely the Oxygen Reduction Reaction (ORR) at the cathode and Hydrogen Oxidation Reaction (HOR) at the anode. They reflect the energy barrier that must be overcome for the reactions to proceed at a given current density. The change in activation overpotential is influenced by the O_2 concentration, which is a function of P_{O2}^{*} as shown in Eq. 19. At a current of 40 A, the reduction percent in activation overpotential approximately attains 5.4% and 6.4% when $P_{O_2}^{in}$ increases from 1 atm to 3 atm, at 55°C and 85°C, respectively. Gerling et al. [45] showed that under controlled O_2 partial pressure conditions, the exchange current density for ORR increased significantly, causing lower activation overpotential at the cathode. Butori et al. [25] decoupled the effects of O_2 partial pressure, humidity, and temperature and found that raising O_2 partial pressure improved voltage stability across current densities by maintaining adequate cathode kinetics even at higher temperatures. On the other hand, increasing $P_{H_2}^{in}$ does not affect the activation overpotential as shown in Figures 7a and 7b at temperatures 55°C and

85°C, respectively. The negligible effect of overpotential with the partial pressure of H_2 is often true in well-optimized PEMFCs under moderate to high H_2 pressures and moderate current densities, where mass-transport losses are not dominant. In other regimes (low H_2 pressure, high current density, degraded diffusion layers, transient operation), the effect can be noticeable [46]. The HOR is often neglected in full cell studies for the sake of simplicity, justified by the high rates of the kinetics [45].

Operating temperature has a significant effect on the activation energy and activation losses of PEMFC. As operating temperature increases, the reaction kinetics improve, mainly due to faster charge transfer reactions, increased proton conductivity in the membrane, and reduced activation energy barrier for the electrochemical reactions. The effect can be understood using the Arrhenius equation, which shows that increasing operating temperature results in higher exchange current density and reduced activation overpotential. The effect of operating temperature is shown in Figures 8a and 8b. When the operating temperature increases from 55°C to 85°C, the percentage decrease of activation overpotential is 7.84% at both O_2 and H_2 supply pressures of 1 atm and 8.82% at both O_2 and H_2 supply pressures of 3 atm

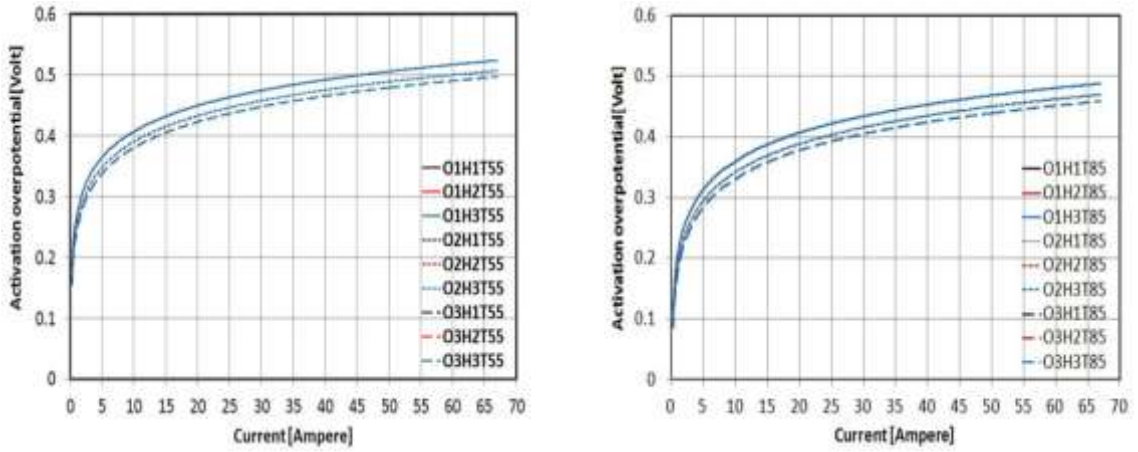

a) b)

Fig. 7. Effect of $P_{O_2}^{in}$ and $P_{H_2}^{in}$ on the activation overpotential at operating temperatures of 55°C and 85°C

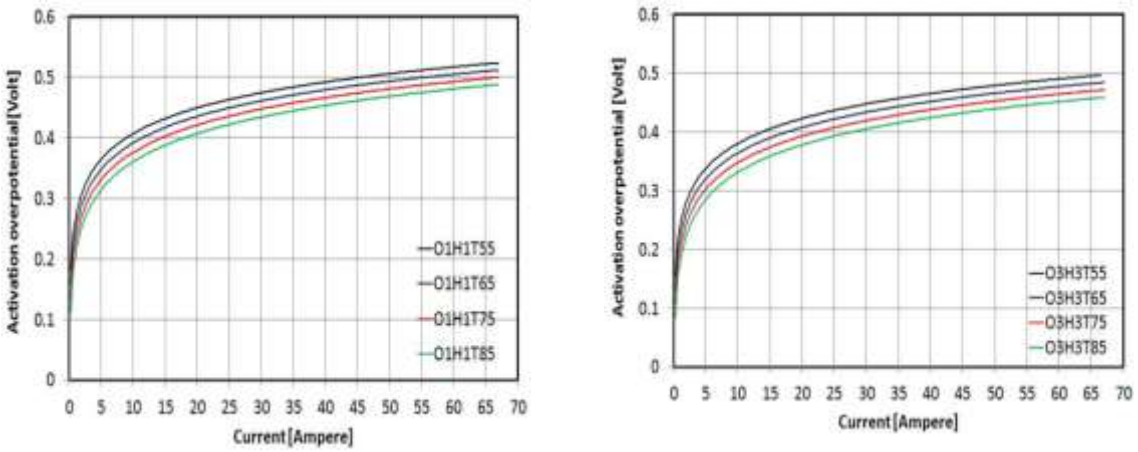

a) b)

Fig. 8. Effect of different operating temperatures on the FC ohmic losses at $P_{O_2}^{in}$ and $P_{H_2}^{in}$ of 1 and 3 atoms

The ohmic overpotentials do not exhibit a pressure term. At higher operating temperatures, water activity and water content of the membrane, and as a result, membrane conductivity increases and ohmic loss decreases [47,48]. Figure 9 indicates that the ohmic losses decrease as the operating temperature increases at all O_2 and H_2 supply pressures. When the operating temperature increases from 55°C to 85°C, the percentage decrease of ohmic losses is 13.5% at all O_2 and H_2 supply pressures.

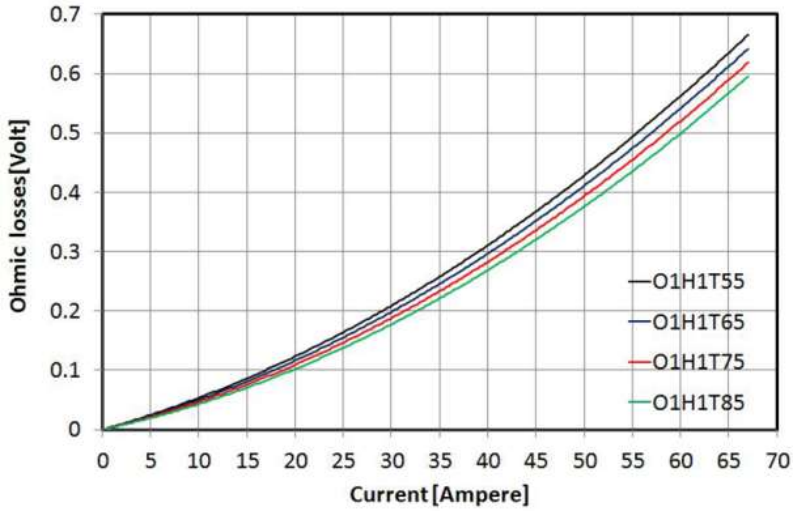

Fig. 9. Effect of different operating temperatures on the FC ohmic losses at all values of $P_{O_2}^{in}$ and $P_{H_2}^{in}$

The cell output voltage depends on the open circuit voltage and overpotentials. The open circuit voltage of a fuel cell depends directly on the reactants' partial pressures, as shown in Eq. 2. When O_2 and H_2 partial pressures increase, the logarithmic term becomes larger, raising the equilibrium cell potential. This reduces the relative magnitude of the overpotential (difference between actual voltage and theoretical voltage). The percentage increase of the Nernst voltage is about 1.3% when $P_{H_2}^{in}$ increases from 1atm to 3 atm at all values of $P_{o_2}^{in}$. On the other hand, the percentage increase of Nernst voltage is about 0.65 % when $P_{O_2}^{in}$ increases from 1atm to 3 atm at all values of $P_{H_2}^{in}$. Increasing either the inlet pressure of H_2 or O_2 can result in a high output voltage, as seen in Figures 10a, 10c,10e, and 10f, and high-power output as shown in Figures 10b, 10d, 10f, and 10g. The increase in the output voltage at a temperature of 55°C when $P_{H_2}^{in}$ Increases from 1 atm to 3 atm approximately attain 3.78%, 3.58%, and 3.48% for $P_{o_2}^{in}$ equal 1 atm, 2 atm, and 3 atm, respectively. These percentages become 3.41%, 3.24%, and 3.15% at an operating temperature of 85°C. The increase in the output voltage at a temperature of 55°C when $P_{O_2}^{in}$ increases from 1 atm to 3 atm approximately attains 8.58%, 8.39%, and 8.27% for $P_{H_2}^{in}$ equal to 1 atm, 2 atm, and 3 atm, respectively. These percentages become 8.21%, 8.04%, and 7.94% at an operating temperature of 85°C.

The effect of increasing $P_{O_2}^{in}$ is more pronounced than that of the H_2. The percentage increase in cell voltage when increasing both $P_{O_2}^{in}$ and $P_{H_2}^{in}$ from 1 atm to 3 atm is 12.37% and 11.63 at operating temperatures of 55°C and 85°C respectively. The same percentage increase applies to the ell output power at all corresponding operating conditions.

Generally speaking, raising the operating pressure could enhance cell performance. Nevertheless, high inlet gas pressure requires more energy from the gas compressor; via

onboard compression, the associated parasitic power can offset these gains beyond an optimal compression level. In the current work, the increase in reactant inlet conditions is achieved by supplying H_2 and O_2 from one of the different storage options, including compressed gas storage and cryogenic storage for H_2 and O_2, metal hydrides for H_2 storage, and chemical O_2 sources [5], which is a commonly adopted configuration for autonomous underwater vehicles (AUVs). Under this assumption, no onboard compressors are required during operation, and therefore, compressor power does not directly influence the instantaneous system performance or the reported efficiency. This energy input occurs off-board during refueling and is not part of the onboard energy balance considered in this study. Each storage option introduces different system-level trade-offs in terms of energy density, thermal management, system complexity, and auxiliary power requirements. A comprehensive evaluation of these storage strategies and their impact on overall system performance is beyond the scope of the present paper. However, this aspect represents an important direction for future research, and it is intended to be addressed in detail in subsequent work.

The effect of operating temperature enhances the fuel cell output voltage and power for all inlet oxygen and hydrogen supply pressures, as shown in Figures 11a to d. When the operating temperature increases from 55°C to 85°C, the increase in the cell output voltage is 14.12% and 13.36% at both $P_{O_2}^{in}$ and $P_{H_2}^{in}$ of 1 and 3 atm, respectively.

On the other hand, open circuit voltage decreases with the increase in operating temperature. As the operating temperature increases, the Gibbs free energy of the reaction decreases (1.229 for standard conditions), leading to a lower Nernst voltage. At the same time, higher temperatures increase the value of RT/2F, which increases the Nernst voltage. This can partially offset the drop caused by the decrease in Gibbs free energy, especially in pressurized operation. In general, the Nernst voltage slightly decreases with temperature under constant pressure. Results show that when the operating temperature increases from 55°C to 85°C, the Nernst voltage decreases 2% and 1.85% at both values of $P_{O_2}^{in}$ and $P_{H_2}^{in}$ of 1 atm, 3 atm, respectively. Finally, decreasing ohmic loss and activation overpotential dominate the Nernst voltage; consequently, the fuel cell performance enhances.

Increases in operating temperature and pressure can improve cell performance, according to experimental research on the impact of operating circumstances on cell performance [30]. Therefore, lowering the irreversibility rate and improving the cell's performance can lower the cost and aid in the fuel cell's commercialization.

5.2. Fuel Cell Stack for AUV

All calculations shown by Eqs. 31 to 36 at maximum predicted cell power under different operating conditions are shown in Table 5. The stack power for the considered AUV is 1523W.

Tab. 5

Different Calculations at Different Operating Conditions

Case	$\dot{W}_{FC,max}$ [W]	I $\dot{W}_{FC,max}$ [Ampere]	N_{FC}	O_2 Cons. [Mole/s]	O_2 Cons. [gm/s]	H_2 Cons. [Mole/s]	H_2 Cons. [gm/s]	η_{Energy}
O1H1T55	16.21	36.5	94	0.0116	0.370	0.022	0.045	0.283
O1H2T55	16.56	37	92	0.0115	0.367	0.022	0.045	0.286

O1H3T55	16.77	37.25	91	0.0114	0.365	0.022	0.044	0.287
O2H1T55	17.01	37.25	90	0.0112	0.359	0.022	0.044	0.291
O2H2T55	17.37	37.75	88	0.0111	0.357	0.021	0.043	0.294
O2H3T55	17.58	38	87	0.0111	0.355	0.021	0.043	0.295
O3H1T55	17.49	37.75	88	0.0111	0.354	0.021	0.043	0.296
O3H2T55	17.85	38.25	86	0.0110	0.352	0.021	0.043	0.298
O3H3T55	18.07	38.25	85	0.0109	0.348	0.021	0.042	0.301
O1H1T65	16.87	37.5	91	0.0114	0.365	0.022	0.044	0.287
O1H2T65	17.24	38	89	0.0113	0.362	0.022	0.044	0.289
O1H3T65	17.46	38.25	88	0.0112	0.360	0.022	0.044	0.291
O2H1T65	17.72	38.5	86	0.0111	0.357	0.021	0.043	0.294
O2H2T65	18.10	38.75	85	0.0110	0.352	0.021	0.043	0.298
O2H3T65	18.32	39	84	0.0109	0.349	0.021	0.042	0.300
O3H1T65	18.23	38.75	84	0.0109	0.349	0.021	0.042	0.300
O3H2T65	18.61	39.25	82	0.0108	0.346	0.021	0.042	0.302
O3H3T65	18.83	39.5	81	0.0108	0.344	0.021	0.042	0.304
O1H1T75	17.57	38.75	87	0.0113	0.362	0.022	0.044	0.289
O1H2T75	17.95	39	85	0.0111	0.357	0.021	0.043	0.294
O1H3T75	18.18	39.25	84	0.0111	0.354	0.021	0.043	0.295
O2H1T75	18.47	39.5	83	0.0110	0.351	0.021	0.043	0.298
O2H2T75	18.86	40	81	0.0109	0.348	0.021	0.042	0.301
O2H3T75	19.09	40	80	0.0107	0.344	0.021	0.042	0.304
O3H1T75	19.01	40	81	0.0108	0.345	0.021	0.042	0.303
O3H2T75	19.40	40.25	79	0.0106	0.341	0.020	0.041	0.307
O3H3T75	19.63	40.5	78	0.0106	0.339	0.020	0.041	0.309
O1H1T85	18.31	39.75	84	0.0111	0.356	0.021	0.043	0.294
O1H2T85	18.70	40	82	0.0110	0.351	0.021	0.043	0.298
O1H3T85	18.93	40.25	81	0.0109	0.349	0.021	0.042	0.300
O2H1T85	19.26	40.5	80	0.0108	0.345	0.021	0.042	0.303
O2H2T85	19.66	41	78	0.0107	0.342	0.021	0.042	0.306
O2H3T85	19.90	41.25	77	0.0106	0.340	0.020	0.041	0.308
O3H1T85	19.83	41	77	0.0106	0.339	0.020	0.041	0.309
O3H2T85	20.23	41.5	76	0.0105	0.337	0.020	0.041	0.311
O3H3T85	20.48	41.75	75	0.0105	0.335	0.020	0.041	0.313

The results indicate a consistent improvement in fuel cell performance with increasing operating temperature and reactant pressures, which is well aligned with findings reported by [30,38,49]. As the temperature rises from 55°C to 85°C, the required number of cells (N_{FC}) decreases significantly (from 94 to 75), reflecting enhanced reaction kinetics and reduced activation losses, as discussed in [49]. A similar trend is observed with increasing O_2 and H_2 pressures, where higher pressurization reduces both oxygen and hydrogen consumption rates due to improved reactant availability and reduced mass transport limitations, consistent with observations by [5]. Moreover, the gradual decrease in reactant consumption indicates better fuel utilization efficiency, which agrees with classical PEMFC performance behavior reported in [50]. The energy efficiency (η_{Energy}) increases from about 0.283 to 0.313, confirming that elevated temperature and pressure enhance overall system efficiency, as also highlighted by [42]. Notably, the best performance was obtained at high temperature (85°C) and high pressures

(O_3H_3). Overall, the present trends are in strong agreement with established literature on PEM fuel cell operation.

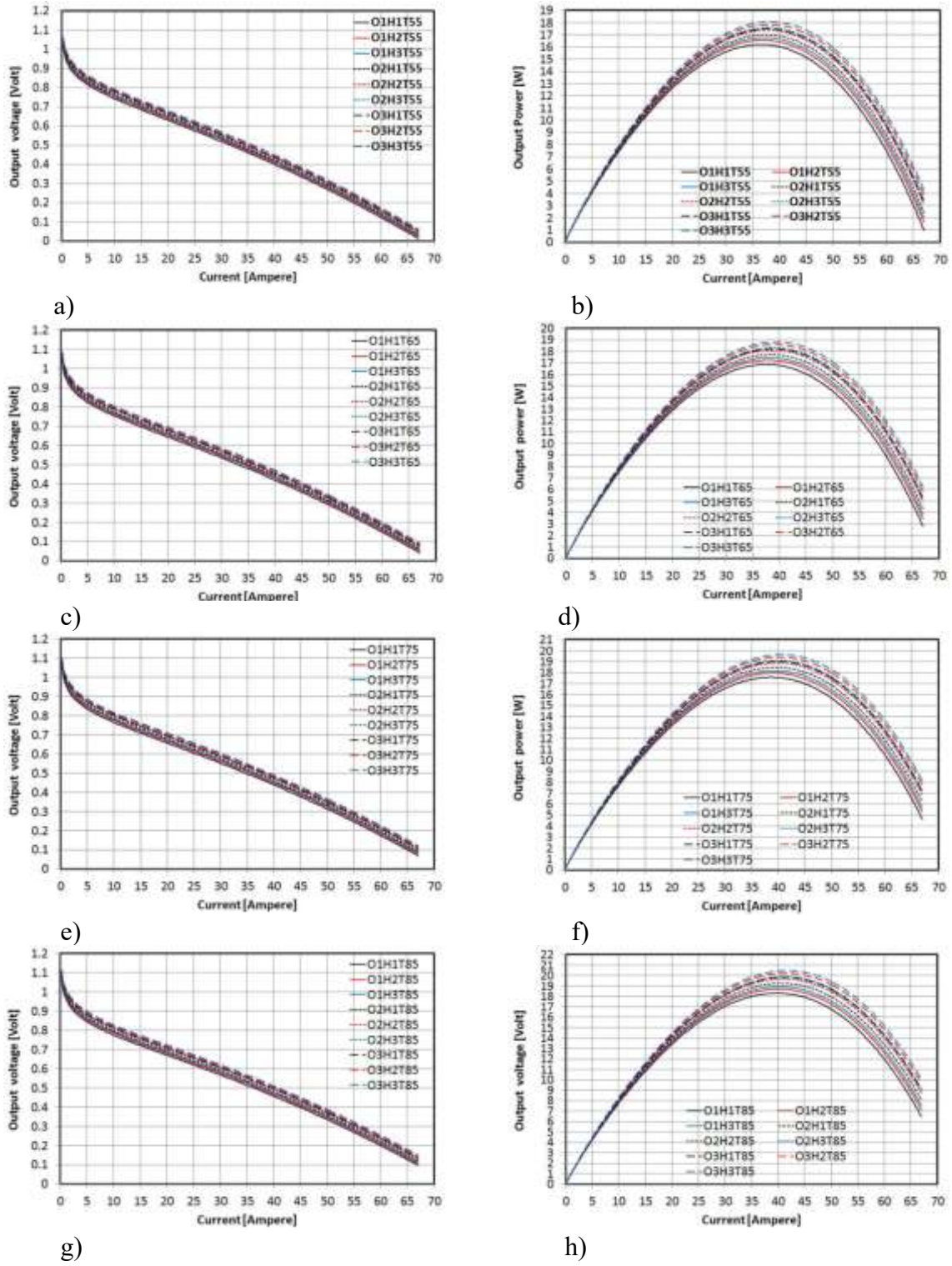

Fig. 10. Effect of $P_{O_2}^{in}$ and $P_{H_2}^{in}$ on the FC output voltage and power at different operating temperatures

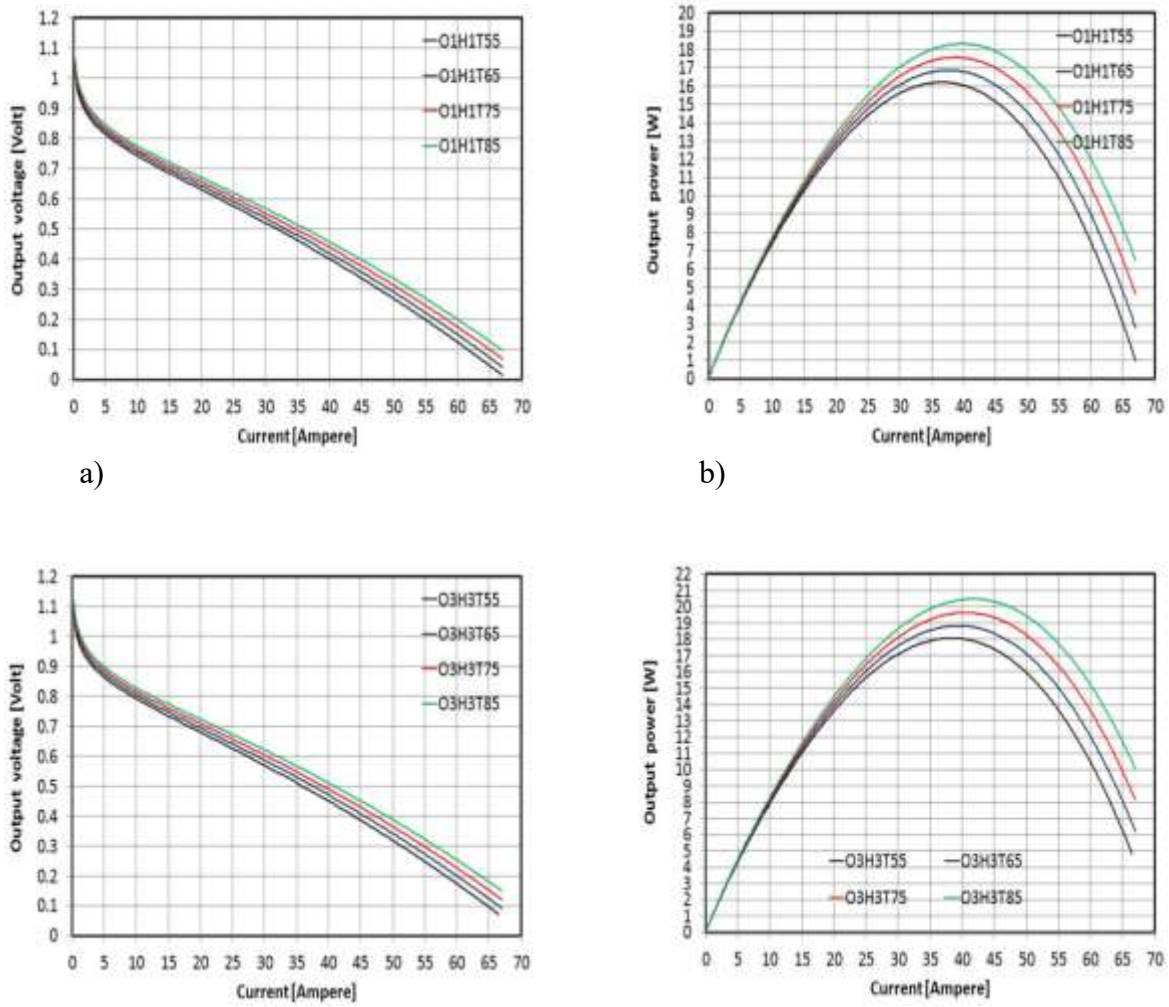

a) b)

c) d)

Fig. 11. Effect of different operating temperatures on the FC output voltage and power at $P_{O_2}^{in}$ and $P_{H_2}^{in}$ of 1 and 3 atoms

Results presented in Table 5 show that increasing operating temperature from 55˚C to 85˚C and increasing both O_2 and H_2 supply pressures from 1 to 3 atm result in:

1. Reduction of the No. of cells from 94 cells at 1 atm to 75 cells for 3 atm, with a decreasing percentage of 20%. The percentage is close to the percentage decrease in fuel cell stack weight and volume.
2. Reduction of the O_2 and H_2 consumptions by 9.5%
3. Increasing the energy efficiency increases by 9.6%

6. CONCLUSIONS

The research methodology entails creating a fuel cell model to predict how different operating conditions affect the performance of a single fuel cell. The impact of operating conditions on cell voltage losses is investigated through a comprehensive investigation. Based on these investigations, size and performance indices are calculated for a fuel cell stack to derive

a commercial AUV under varying operating conditions. The following conclusions can be made in light of this study:

- The higher H_2 and O_2 supply pressures increase cell performance mainly due to the decrease in activation overpotential at all current densities and operating temperatures. On the other hand, they do not affect the ohmic losses.
- Increasing the cell operating temperature results in better fuel cell performance, mainly due to the decrease in both ohmic and activation losses at all current densities and gas supply pressures.
- The effect of increasing $P_{O_2}^{in}$ on the FC performance is more pronounced than that of and $P_{H_2}^{in}$.
- As $P_{O_2}^{in}$ increases from 1 atm to 3 atm at a current density of 40 A, the reduction in activation overpotential approximately attains 5.4% and 6.4%, at 55°C and 85°C, respectively.
- The ohmic losses decrease as the operating temperature increases at both values of $P_{O_2}^{in}$ and $P_{H_2}^{in}$ of 1 and 3 atm respectively (ohmic losses is 13.5% at operating temperature increases from 55°C to 85°C).
- Concerning the FC stack for the assigned AUV, the increase of operating temperature from 55°C to 85°C and the increase of both O_2 and H_2 supply pressures from 1 to 3 atm result in a reduction of the number of cells by 20%. This proportion is comparable to the fuel cell stack weight and volume reduction, with a 9.5% decrease in O_2 and H_2 consumptions leading to an increase in the energy efficiency by 9.6%.

References

1. Wang Z., Z. Liu, L. Fan, Q. Du, K. Jiao. 2023. „Application progress of small-scale proton exchange membrane fuel cell''. *Energy Reviews* 2: 10017. ISSN: 2772-9702. DOI: https://doi.org/10.1016/j.enrev.2023.100017.
2. Chang X., T. Ma, R. Wu. 2019. „Impact of urban development on residents' public transportation travel energy consumption in China: An analysis of hydrogen fuel cell vehicles alternatives". *International Journal of Hydrogen Energy* 44: 16015-27. ISSN: 1879-3487. DOI: https://doi.org/10.1016/j.ijhydene.2018.09.099.
3. Carrette L., K.A. Friedrich, U. Stimming. 2001. „Fuel cells - fundamentals and applications". *Fuel Cells* 1(1): 5-39. ISSN: 1615-6854. DOI: https://doi.org/10.1002/1615-6854(200105)1:1<5::AID-FUCE5>3.0.CO;2-G.
4. Duong, V., N.H. Hiep. 2025. „Hybrid propulsion based on fuel cells". *DTU Journal of Science and Technology* 01(68): 3-15. ISSN: 1858-4905.
5. D'Amore-Domenech R., M.A. Raso, A. Villalba-Herreros, Ó. Santiago, E. Navarro, T.J. Leo. 2018. „Autonomous underwater vehicles powered by fuel cells: Design guidelines". *Ocean Engineering* 153: 387-98. ISSN: 0029-8018. DOI: https://doi.org/10.1016/j.oceaneng.2018.01.117.
6. Sawa T., T. Aoki, I. Yamamoto, S. Tsukioka, H. Yoshida, T. Hyakudome, et al. 2005. „Performance of the fuel cell underwater vehicle URASHIMA". *Acoustical Science and Technology* 26(3): 249-56. ISSN: 1346-3962. DOI: https://doi.org/10.1250/ast.26.249.
7. Hasvold Ø., N.J. Størkersen, S. Forseth, T. Lian. 2006. „Power sources for autonomous underwater vehicles". *Journal of Power Sources* 162: 935-42. ISSN: 0378-7753. DOI: https://doi.org/10.1016/j.jpowsour.2005.07.021.

8. Waseem Mohammad, Mohammad Amir, G.S. Lakshmi, S. Harivardhagini, Mumtaz Ahmad. 2023. "Fuel Cell-Based Hybrid Electric Vehicles: An Integrated Review of Current Status, Key Challenges, Recommended Policies, and Future Prospects". *Green Energy and Intelligent Transportation* 2: 100121. ISSN: 2097-2512. DOI: https://doi.org/10.1016/j.geits.2023.100121.
9. Weydahl H., M. Gilljam, T. Lian, T.C. Johannessen, S.I. Holm, J.Ø. Hasvold. 2020. „Fuel cell systems for long-endurance autonomous underwater vehicles – challenges and benefits". *International Journal of Hydrogen Energy* 45: 5543-53. ISSN: 1879-3487. DOI: https://doi.org/10.1016/j.ijhydene.2019.05.035.
10. Farahabadi H.B., M.R. Firuzjaei, A.M. Mir, R. Youneszadeh. 2023. „Fuel cell power system conceptual design for unmanned underwater vehicles". *Hydrogen, Fuel Cell & Energy Storage* 10: 33-50. ISSN: 2980-8537. DOI: https://doi.org/10.22104/IJHFC.2022.5884.1248.
11. Cai Q., D.J.L. Brett, D. Browning, N.P. Brandon. 2010. „A sizing-design methodology for hybrid fuel cell power systems and its application to an unmanned underwater vehicle". *Journal of Power Sources* 195: 6559-69. ISSN: 0378-7753. DOI: https://doi.org/10.1016/j.jpowsour.2010.04.078.
12. Sahoo A., S.K. Dwivedy, P.S. Robi. 2019. „Advancements in the field of autonomous underwater vehicle". *Ocean Engineering* 181: 145-60. ISSN: 0029-8018. DOI: https://doi.org/10.1016/j.oceaneng.2019.04.011.
13. Xiang X., C. Yu, Q. Zhang, P.A. Wilson, G. Xu. 2020. „Maneuvering-based actuation evaluation of an AUV with control surfaces and through-body thrusters". *Applied Ocean Research* 96: 102046. ISSN: 0141-1187. DOI: https://doi.org/10.1016/j.apor.2019.102046.
14. Monterroso Muñoz A., M.J. Moron-Fernández, D. Cascado-Caballero, F. Diaz-del-Rio, P. Real. 2023. „Autonomous Underwater Vehicles: Identifying Critical Issues and Future Perspectives in Image Acquisition". *Sensors* 23: 4986. ISSN: 1424-8220. DOI: https://doi.org/10.3390/s23104986.
15. Loshchenkov V.V.K.V. 2024. „Fuel Cells for AUV Power Supply". In: *International Conference on Ocean Studies ICOS*. 08-11 October 2024, Vladivostok, Russian Federation. DOI: 10.1109/ICOS63634.2024.10775586.
16. Mendez A., T.J. Leo, M.A. Herreros. 2014. „Current state of technology of fuel cell power systems for autonomous underwater vehicles". In: *1st International e-conference Energies*. 14-32 March 2014. MDPI: Basel, Switzerland. DOI: https://doi:10.3390/ece-1-d001.
17. Mendez A., T.J. Leo, M.A. Herreros. 2014. „Current state of technology of fuel cell power systems for autonomous underwater vehicles". *Energies* 7: 4676-93. ISSN: 1996-1073. DOI: https://doi.org/10.3390/en7074676.
18. Pielecha I. 2022. „Modeling of fuel cells characteristics in relation to real driving conditions of FCHEV vehicles". *Energies* 15: 6753. ISSN: 1996-1073. DOI: https://doi.org/10.3390/en15186753.
19. Tsukioka S., T. Aoki, I. Yamamoto, H. Yoshida, T. Hyakudome, T. Sawa, et al. 2005. „The PEM fuel cell system for autonomous underwater vehicles". *Marine Technology Society Journal* 39(3): 56-64. ISSN: 0025-3324. DOI: https://doi.org/10.4031/002533205787442558.

20. Fakhreddine O., Y. Gharbia, J.F. Derakhshandeh, A.M. Amer. 2023. „Challenges and solutions of hydrogen fuel cells in transportation systems: a review and prospects". *World Electric Vehicle Journal* 14: 156. ISSN: 2032-6653. DOI: https://doi.org/10.3390/wevj14060156.
21. Deutsch C., A. Chiche, S. Bhat, C. Lagergren, G. Lindbergh, and J. Kuttenkeuler. 2022. „Evaluation of energy management strategies for fuel cell/battery-powered underwater vehicles against field trial data". *Energy Conversion and Management X* 14: 100193. ISSN: 2590-1745. DOI: https://doi.org/10.1016/j.ecmx.2022.100193.
22. Mann R.F., J.C. Amphlett, M.A.I. Hooper, H.M. Jensen, B.A. Peppley, P.R. Roberge. 2000. „Development and application of a generalized steady-state electrochemical model for a PEM fuel cell". *Journal of Power Sources* 86: 173-80. ISSN: 0378-7753. DOI: https://doi.org/10.1016/S0378-7753(99)00484-X.
23. Corrêa J.M., S. Member, F.A. Farret, L.N. Canha, M.G. Simões. 2004. „An electrochemical-based fuel-cell model suitable for electrical engineering automation approach". *IEEE Transactions on Industrial Electronics* 51(5): 1103-12. ISSN: 0278-0046. DOI: https://doi.org/10.1109/TIE.2004.834972.
24. Abdin Z., C.J. Webb, E.M. Gray. 2016. „PEM fuel cell model and simulation in Matlab-Simulink based on physical parameters". *Energy* 116: 1131-44. ISSN: 0360-5442. DOI: https://doi.org/10.1016/j.energy.2016.10.033.
25. Butori M., Björn Eriksson, Nikola Nikolic, Carina Lagergren, Goran Lindbergh, Rakel Wreland Lindstrom. 2023. "The effect of oxygen partial pressure and humidification in proton exchange membrane fuel cells at intermediate temperature (80-120°C)". *Journal of Power Sources* 563: 232803. ISSN: 0378-7753. DOI: https://doi.org/10.1016/j.jpowsour.2023.232803.
26. Ali M.A., M.E. Mandour, M.E. Lotfy. 2023. „Adaptive Estimation of Quasi-Empirical Proton Exchange Membrane Fuel Cell Models Based on Coot Bird Optimizer and Data Accumulation". *Sustainability* 15: 9071. ISSN: 2071-1050. DOI: https://doi.org/10.3390/su15119017.
27. Pukrushpan J.T., H. Peng, A.G. Stefanopoulou. 2004. "Control-oriented modeling and analysis for automotive fuel cell". *Journal of Dynamic Systems, Measurement, and Control* 126: 14-25. ISSN: 0022-0434. DOI: https://doi.org/10.1115/1.1648308.
28. Correa J.M., F.A. Farret, M.G. Simoes. 2005. „Sensitivity analysis of the modeling parameters used in simulation of proton exchange membrane fuel cells". *IEEE Transactions on Energy Conversion* 20(1). ISSN: 0885-8969. DOI: https://doi.org/10.1109/TEC.2004.842382.
29. Jia J., Q. Li, Y. Wang, S. Member, Y.T. Cham, S. Member, et al. 2009. „Modeling and dynamic characteristic simulation of a proton exchange membrane fuel cell". *IEEE Transactions on Energy Conversion* 24(1): 283-91. ISSN: 0885-8969. DOI: https://doi.org/10.1109/TEC.2008.2011837.
30. Miansari M., K. Sedighi, M. Amidpour, E. Alizadeh, M. Miansari. 2009. „Experimental and thermodynamic approach on proton exchange membrane fuel cell performance". *Journal of Power Sources* 190: 356-61. ISSN: 0378-7753. DOI: https://doi.org/10.1016/j.jpowsour.2009.01.082.
31. Barelli L., G. Bidini, F. Gallorini, A. Ottaviano. 2010. „Analysis of the operating conditions influence on PEM fuel cell performances by means of a novel semi-empirical model". *International Journal of Hydrogen Energy* 36: 10434-42. ISSN: 1879-3487. DOI: https://doi.org/10.1016/j.ijhydene.2010.06.032.

32. Haji Shaker. 2011. „Analytical modeling of PEM fuel cell I-V curve". *Renewable Energy* 36: 451-58. ISSN: 0960-1481. DOI: https://doi.org/10.1016/j.renene.2010.07.007.
33. El-Monem A.A.A., A.M. Azmy, S.A. Mahmoud. 2014. „Effect of process parameters on the dynamic behavior of polymer electrolyte membrane fuel cells for electric vehicle applications". *Ain Shams Engineering Journal* 5: 75-84. ISSN: 2090-4479. DOI: https://doi.org/10.1016/j.asej.2013.05.001.
34. Alrewq M., A. Albarbar. 2016. „Investigation into the characteristics of proton exchange membrane fuel cell-based power system". *IET Science, Measurement & Technology* 10: 200-206. ISSN: 1751-8822. DOI: https://doi.org/10.1049/iet-smt.2015.0046.
35. Ceraolo M., C. Miulli, A. Pozio. 2003. „Modeling static and dynamic behaviour of proton exchange membrane fuel cells on the basis of electrochemical description". *Journal of Power Sources* 113: 131-44. ISSN: 0378-7753. DOI: https://doi.org/10.1016/S0378-7753(02)00565-7.
36. Qasem N.A.A., Gubran A.Q. Abdulrahman. 2024. „A recent comprehensive review of Fuel Cells: history, types, and applications". *International Journal of Energy Research* 2024. ISSN: 0363-907X. DOI: https://doi.org/10.1155/2024/7271748.
37. Amphlett J.C., R.M. Baumert, R.F. Mann, B.A. Peppley, P.R. Roberge, T.J. Harris. 1995. „Performance modeling of the Ballard Mark IV solid polymer electrolyte fuel cell; I. mechanistic model development". *Journal of the Electrochemical Society* 142(1): 1-8. ISSN: 0013-4651. DOI: https://doi.org/10.1149/1.2043866.
38. Amphlett J.C., R.M. Baumert, R.F. Mann, B.A. Peppley, P.R. Roberge, T.J. Harris. 1995. „Performance modeling of the Ballard Mark IV solid polymer electrolyte fuel cell; II. empirical model development". *Journal of the Electrochemical Society* 142: 9-15. ISSN: 0013-4651. DOI: https://doi.org/10.1149/1.2043959.
39. Pathapati P.R., X. Xue, J. Tang. 2005. „A new dynamic model for predicting transient phenomena in a PEM fuel cell system". *Renewable Energy* 30: 1-22. ISSN: 0960-1481. DOI: https://doi.org/10.1016/j.renene.2004.05.001.
40. Gasparoto H.F., O. Chocron, M. Benbouzid, P.S. Meirelles. 2021. „Advances in reconfigurable vectorial thrusters for adaptive underwater robots". *Journal of Marine Science and Engineering* 9: 170. ISSN: 2077-1312. DOI: https://doi.org/10.3390/jmse9020170.
41. Chakrabarti Subrata K. 2005. "Loads and Responses. In Handbook of Offshore Engineering", edited by Chakrabarti Subrata K., 133-196. Elsevier Science. ISBN: 978-0-08-044381-2. DOI: https://doi.org/10.1016/B978-008044381-2.50007-2.
42. Barbir Frano. 2013. *PEM Fuel cells: Theory and practice*. Academic Press is an imprint of Elsevier. ISBN: 978-0-12-387710-9.
43. Hoeflinger J., P. Hofmann. 2020. „Air mass flow and pressure optimisation of a PEM fuel cell range extender system". *International Journal of Hydrogen Energy* 45: 29246-58. ISSN: 1879-3487. DOI: https://doi.org/10.1016/j.ijhydene.2020.07.176.
44. Chitsaz A., M.A. Haghghi, J. Hosseinpour. 2019. „Thermodynamic and exergoeconomic analyses of a proton exchange membrane fuel cell (PEMFC) system and the feasibility evaluation of integrating with a proton exchange membrane electrolyzer (PEME)". *Energy Conversion and Management* 186: 487-99. ISSN: 0196-8904. DOI: https://doi.org/10.1016/j.enconman.2019.03.004.
45. Gerling C., Matthias Hanauer, Ulrich Berner, K. Andreas Friedrich. 2022. „PEM Single Cells under Differential Conditions: Full Factorial Parameterization of the ORR and HOR Kinetics and Loss Analysis". *Journal of The Electrochemical Society* 169: 014503. ISSN: 0013-4651. DOI: https://doi.org/10.1149/1945-7111/ac44ba.

46. Stühmeier B.M., M.R. Pietsch, J. Schwämmlein, H.A. Gasteiger. 2021. „Pressure and temperature dependence of the hydrogen oxidation and evolution reaction kinetics on Pt electrocatalysts via PEMFC-based Hydrogen-Pump Measurements". *Journal of the Electrochemical Society* 168: 064516. ISSN: 0013-4651. DOI: https://doi.org/10.1149/1945-7111/ac099c.
47. Askaripour H. 2019. „Effect of operating conditions on the performance of a PEM fuel cell". *International Journal of Heat and Mass Transfer* 144: 118705. ISSN: 0017-9310. DOI: https://doi.org/10.1016/j.ijheatmasstransfer.2019.118705.
48. Zhang J., H. Zhang, J. Wu, J. Zhang. 2013. "PEM Fuel Cell Testing and Diagnosis". Elsevier B.V. ISBN: 978-0-444-53688-4. DOI: https://doi.org/10.1016/B978-0-444-53688-4.00004-8.
49. EG&G Technical Services Inc. 2004. *Fuel Cell Handbook*. 7th ed. U.S. Department of Energy. Under Contract No. DE-AM26-99FT40575.
50. Dicks A.L., D.A.J. Rand. 2018. *Fuel Cell Systems Explained*. 3rd ed. John Wiley & Sons Ltd. ISBN: 9781118706978.

Received 09.01.2026; accepted in revised form 04.05.2026